Available online at www.sciencedirect.com

ScienceDirect

Proceedings of the Combustion Institute 35 (2015) 2101–2108

Proceedings of the Combustion Institute

www.elsevier.com/locate/proci

Cavity ignition in supersonic flow by spark discharge and pulse detonation

Timothy M. Ombrello [a,*], Campbell D. Carter [a], Chung-Jen Tam [b], Kuang-Yu Hsu [c]

[a] U.S. Air Force Research Laboratory, Wright-Patterson Air Force Base, OH 45433, USA
[b] Taitech, Beavercreek, OH 45430, USA
[c] Innovative Scientific Solutions, Inc., Dayton, OH 45459, USA

Available online 18 August 2014

Abstract

Ignition of an ethylene fueled cavity in a supersonic flow was achieved through the application of two energy deposition techniques: a spark discharge and pulse detonator (*PD*). High-frequency shadowgraph and chemiluminescence imaging showed that the spark discharge ignition was passive with the ignition kernel and ensuing flame propagation following the cavity flowfield. The *PD* produced a high-pressure and temperature exhaust that allowed for ignition at lower tunnel temperatures and pressures than the spark discharge, but also caused significant disruption to the cavity flowfield dynamics. Under certain cavity fueling conditions a multiple regime ignition process occurred with the *PD* that led to decreased cavity burning and at times cavity extinction. Simulations were performed of the *PD* ignition process, capturing the decreased cavity burning observed in the experiments. The *PD* exhaust initially ignited and burned the fuel within the cavity rapidly. Simultaneously, the momentary elevated pressure from the detonation caused a blockage of the cavity fuel, starving the cavity until the *PD* completely exhausted and the flowfield could recover. With sufficiently high cavity fueling, the decrease in burning during the *PD* ignition process could be mitigated. Cavity fuel injection and entrainment of fuel through the shear layer from upstream injection allowed for the spark discharge ignition process to exhibit similar behavior with peaks and valleys of heat release (but to a lesser extent). The results of using the two energy deposition techniques emphasized the importance of cavity fueling and flowfield dynamics for successful ignition.
Published by Elsevier Inc. on behalf of The Combustion Institute.

Keywords: Scramjet; Cavity ignition; Supersonic combustion; Pulse detonation

1. Introduction

Successfully igniting high-speed air-breathing combustors, such as supersonic combustion ramjets, is a significant challenge because of the restrictive reactive environment. While the limited residence times in these combustors can be mitigated through the use of cavities and struts [1,2],

* Corresponding author. Address: 1950 Fifth Street, Building 18A, Wright-Patterson AFB, OH, USA. Fax: +1 937 656 4659.
E-mail address: timothy.ombrello.1@us.af.mil (T.M. Ombrello).

http://dx.doi.org/10.1016/j.proci.2014.07.068
1540-7489/Published by Elsevier Inc. on behalf of The Combustion Institute.

the low pressures and temperatures in the supersonic flow at takeover flight speeds (Mach numbers <5) prohibit auto-ignition. Therefore energy addition techniques typically need to be applied to produce elevated local temperatures, elevated pressures, or radical rich effluents for ignition. While the end result of igniting a supersonic flowpath is self-sustained heat release, directly achieving this can be energy intensive because of the need to engage a significant quantity of the fuel. An alternative is to ignite a small fraction of the fuel, such as in a cavity, which provides flameholding and a source of high temperatures to engage the remainder of the fuel in the flow.

Historically, these techniques have ranged from pure electrical energy addition via low- and high-frequency pulsed discharges [3,4] and plasma jets/torches [5–7], to a combination of electrical and chemical energy addition via fueled torches.[8] While pure electrical energy addition is attractive because of its simplicity, it is conceivable that considerable electrical energy would be required. For example, consider differences between a plasma torch and a fueled torch. A plasma torch produces a plume with very high temperatures that is rich in radicals but may require 10 s of kJ of electrical energy input. A fueled torch has minimal initial ignition energy (typically) and relies upon chemical heat release from a fuel while achieving similar plume characteristics. Therefore, utilizing chemical energy for an ignition device is attractive from a system level perspective.

Chemical energy from a fuel can be extracted in many ways and includes combustion at constant pressure, constant volume, through a detonation, or some combination. While a deflagration (flame) through constant volume combustion can provide rapid heat release and elevated pressures, a detonation is superior because of the coupling between the shock and reaction front. For example, a simple C_3H_8/air reactive system starting at 101 kPa and 300 K results in a constant volume combustion temperature (T) of 2631 K and a pressure (P) of 943 kPa, while a detonation at Chapman–Jouguet conditions results in a T of 2807 K and a P of 1773 kPa. Therefore, a detonation, which produces a high-T and P plume that is rich in radicals, provides some of the most important ingredients for successful ignition.

The goal of the present study was to investigate cavity ignition in a supersonic flow using two forms of energy addition: a spark discharge and a pulse detonator (PD). The spark discharge provided a small pure electrical energy addition technique for ignition with minimal disruption, while the PD provided a chemical heat release technique, with a disruptive plume of high-P, T, and velocity gas. These processes were investigated with high-bandwidth shadowgraph and chemiluminescence imaging, as well as detailed reactive flow simulations, in order to understand the complex flow interactions.

2. Experimental setup

The experiments were performed in the supersonic wind tunnel of Research Cell 19 at Wright-Patterson Air Force Base [9]. For the current experiments, a generic cavity configuration was used (Fig. 1); the entire flowpath is 15.2 cm wide, and there are two ports in the base of the cavity located 1.9 cm on either side of the symmetry plane to accommodate both the spark discharge and PD ignition devices [2]. While there are many potential locations for the ignition devices in and around the cavity, the current choice was motivated by where a spark igniter has been used successfully for many years and thus was a good starting point for comparison of cavity ignition with the two devices. Fuel (C_2H_4) was injected into the cavity from eleven holes in the cavity closeout ramp and for some of the experiments through a 2.5 cm wide slot 18.4 cm upstream of the cavity. Since the fueling was symmetric with respect to the span wise distribution, the mixture should be the same at the location of both ignition devices. Other experiments that have been performed showed that there was no major asymmetry in the cavity in terms of ignition. A flow Mach number (M) of 2, corresponding to a flight value of M_{flight} ≈4, total temperature (T_0) of 600 K and total pressure (P_0) of 483 kPa were used for all experiments.

High-frame-rate shadowgraph and chemiluminescence imaging were used to characterize the transient ignition process, with both techniques providing an integrated view, in this case across the span of the cavity. For the shadowgraphy, the illumination source was an Hg–Xe lamp where the light was collimated, passed through the flow path, and then impinged upon a sheet of frosted glass. The shadowgraph image on the frosted glass was then captured by a Photron SA5 CMOS camera at 100,000 frames per second and a resolution of 320 × 192 pixels. All shadowgraphs were normalized with (i.e., divided by) a time-averaged image taken under quiescent conditions (no tunnel

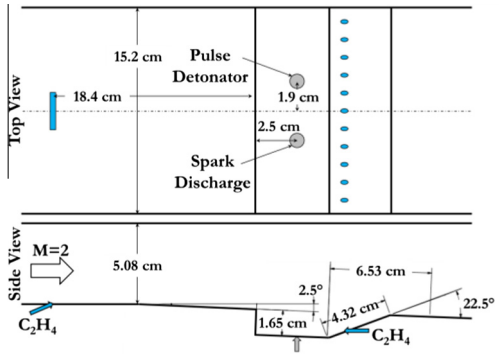

Fig. 1. Schematic of cavity based flow path.

flow), a step that dramatically improves image quality. Chemiluminescence (primarily from CH^* and C_2^*, with soot emission inhibited by high fuel–air mixing rates) was collected from the same field of view as the shadowgraph.

A simple automotive style spark ignition system and plug was used to provide a single 10 mJ/pulse of energy for the spark discharge. The *PD* was comprised of a 61-cm-long and 1.03-cm-ID stainless steel tube with compression fittings. The fuel (C_3H_8) and oxidizer (N_2O) were chosen to produce detonations in the small diameter tube and at the static pressure in the tunnel. The PD tube was overfilled with the reactive mixture to ensure that a detonation reached the cavity. The excess reactants that were injected into the cavity from overfilling prior to the detonation emerging were found to not change the cavity ignition process. The reactive mixture in the PD was ignited with the same automotive spark discharge and each firing produced a detonation wave with near Chapman–Jouguet conditions. In contrast to the spark discharge, the energy released from each detonation was ~100 J. While the *PD* could be operated at greater than 10 Hz repetition rate, single firings were used for the cavity ignition study. More details are provided in Ref. [10].

3. Results

3.1. Shadowgraph and chemiluminescence

The spark discharge and *PD* produced very different cavity ignition processes because of how they deposit energy and interact with the flow. The ignition process with a spark discharge relies heavily upon the cavity flowfield to spread the initial flame kernel and therefore is classified as a *passive* device. On the other hand, a detonation is disruptive to the cavity flow but still relies upon the cavity dynamics to sustain the flame. Because of the interaction of the ignition devices with the flow, the cavity burning depended strongly on the fueling condition. To best capture the ignition process with these two devices, shadowgraphy allowed for interrogation of the density fluctuations and chemiluminescence imaging provided a pseudo marker of the heat release. While the measurements were not taken simultaneously, good repeatability between each ignition sequence allowed for meaningful comparison between the shadowgraph and chemiluminescence imaging.

A representative set of images from the high-frame-rate videos for both ignition devices are shown in Fig. 2 with a fueling rate from the slot upstream of the cavity (Q_{slot}) of 144 slpm (standard liters/min) and 104 slpm from the holes in the cavity closeout ramp (Q_{cavity}). Chemiluminescence images are displayed in *false-color* to provide good contrast. For the spark discharge, the ignition kernel is present in the shadowgraph image by 0.01 ms based on the observed density gradients but is difficult to see with chemiluminescence because, presumably, the heat release is low. By 0.09 ms the ignition kernel had moved towards the front of the cavity, following the recirculation pattern, but had grown little. In stark contrast, when the *PD* was fired into the cavity under the same conditions, the cavity disruption was dramatic. Within 0.01 ms, the detonation plume had reached the shear layer because of the high velocity (~2000 m/s) exiting the tube. While the detonation had significant momentum flux that filled the cavity rapidly, it was isolated to the cavity and downstream (i.e., little upstream propagation). Furthermore, the initial detonation plume reached halfway across the core flow above the cavity by 0.09 ms.

Later in time, the distinct difference in the cavity ignition process becomes clearer (Fig. 3). Within 1 ms, the ignition kernel from the spark discharge had grown and moved to the front of the cavity and was being entrained into the shear layer. This allowed for rapid circulation of the combustion products towards the end of the cavity and then down the ramp to ignite the fuel by 2–2.5 ms. At that point, the cavity gases had completed one *cycle*, and there was significant heat release. In shadowgraph images, this was shown by the thickening and movement of the shear layer that created a shock at the front edge of the cavity (starting at ~1–1.5 ms). By 3 ms, the cavity appeared to be in a stable/steady state burning process with a shear layer flame, as well as burning within the cavity. On the other hand for the *PD*, the strong detonation plume had significantly decayed by 1 ms, and there was the appearance of cavity burning and a strong shock at the front edge of the cavity. By 3 ms, the cavity burning had decreased and the *PD* was nearing the end of its exhaust process. This resulted in less heat release in the cavity, as shown by the weaker shock at the front edge of the cavity. At this point, the large disruption from the detonation had significantly affected the cavity cycling and therefore changed the burning process.

The cavity burning for the spark discharge changed little between 3 and 4 ms (Figs. 3 and 4) and also did not change significantly thereafter. Therefore, 3 ms after the spark discharge, the cavity had settled into a quasi-stable burning process that appeared to be independent of the ignition event. This makes sense since the cavity had cycled a couple of times (~ 1–1.5 ms/cycle). For the *PD*, on the other hand, the cavity burning steadily decreased between 3 and 5 ms and indeed appeared nearly extinguished at 5 ms before achieving quasi-stable burning at approximately 8 ms. While the cavity was successfully ignited using both devices, the processes were vastly different.

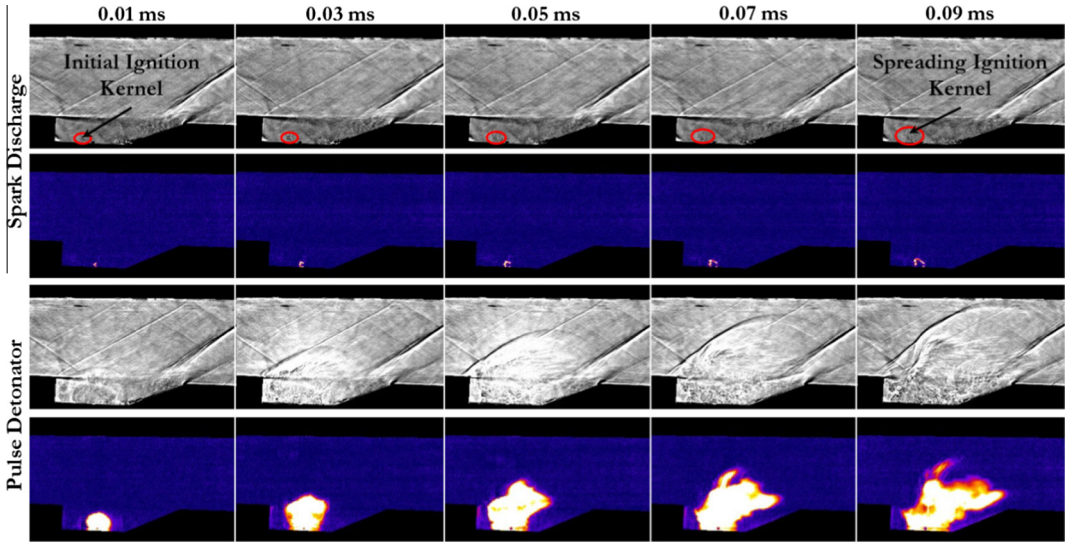

Fig. 2. Shadowgraph and chemiluminescence images of spark discharge and *PD* cavity ignition for $Q_{slot}/Q_{cavity} = 144/104$ slpm from 0.01 to 0.09 ms.

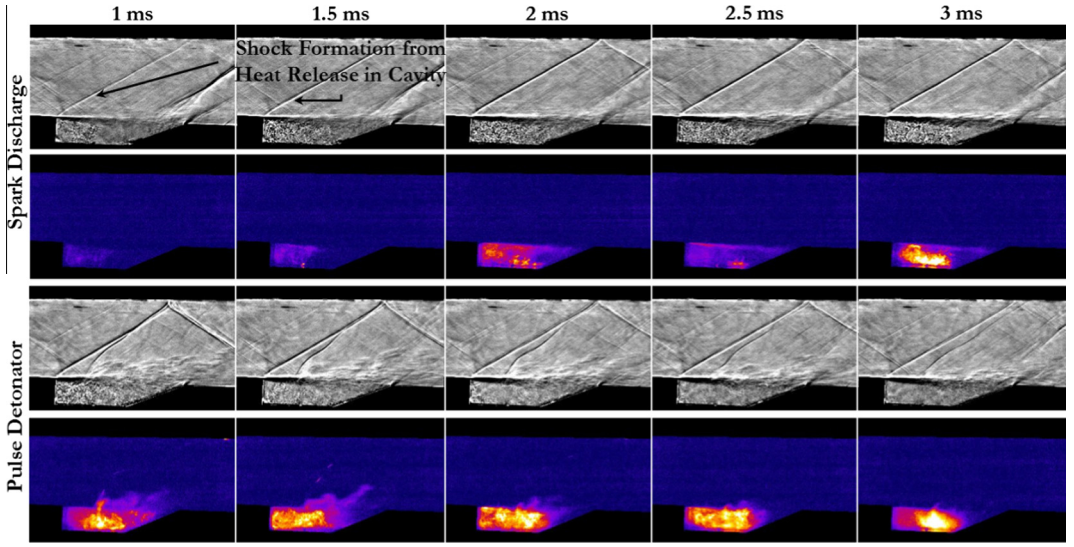

Fig. 3. Shadowgraph and chemiluminescence images of spark discharge and *PD* cavity ignition for $Q_{slot}/Q_{cavity} = 144/104$ slpm from 1 to 3 ms.

In an attempt to go beyond simple qualitative images, the total chemiluminescence from the cavity versus time was plotted. A control volume of the cavity only was used for the measurement, and Fig. 5 shows the results for the spark discharge and the *PD* with $Q_{slot}/Q_{cavity} = 0/66$ slpm. The images were normalized to the peak chemiluminescence coming from the *PD*. The total emission, and hence heat release in the cavity, followed different paths for the two ignition devices, but it converged to the same level by approximately 8 ms. The heat release from spark discharge ignition was gradual with a local peak at 4 ms, while the *PD* had five distinct regimes (shown by the numbering in Fig. 5). Initially there was significant emission (regime I), from *PD* chemiluminescence and soot incandescence, followed by a rapid decay and then a diminished and relatively constant level of emission (regime II). The duration of regime II was approximately one cavity cycle time that led to a "cavity ignition delay time." In regime III, there was a rapid

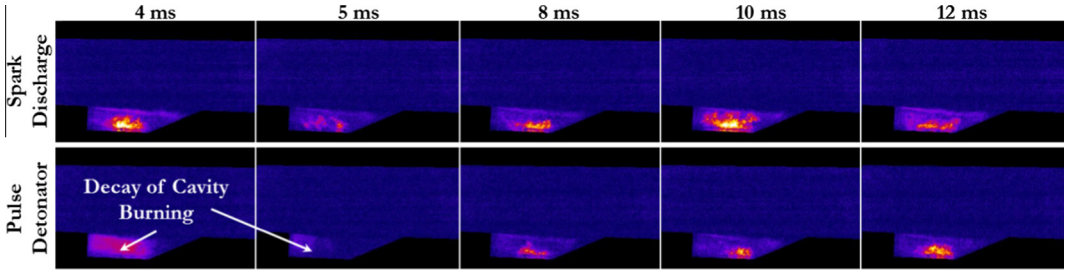

Fig. 4. Chemiluminescence images of spark discharge and *PD* cavity ignition for $Q_{slot}/Q_{cavity} = 144/104$ slpm from 4 to 12 ms.

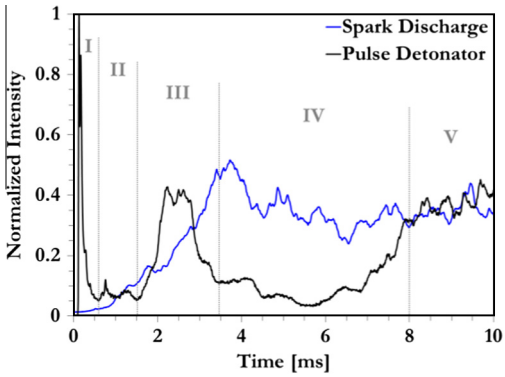

Fig. 5. Average integrated chemiluminescence in cavity during ignition versus time with $Q_{slot}/Q_{cavity} = 0/66$ slpm for spark discharge and *PD*.

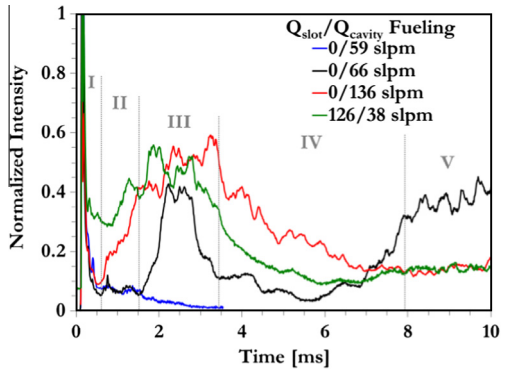

Fig. 6. Average integrated chemiluminescence in cavity during ignition versus time for *PD* at different Q_{slot} and Q_{cavity}.

increase in heat release from burning the fuel in the cavity. Once the fuel was consumed, there was a long lull in integrated emission of 3–4 ms (regime IV) that was needed to replenish a combustible mixture. At that point (regime V), the heat release in the cavity increased to a quasi-steady value that was independent of the ignition event.

When different fuel flow rates in the cavity were used, the distinct burning regimes changed dramatically. In Fig. 6, the result with $Q_{slot}/Q_{cavity} = 0/66$ slpm was compared to that with $Q_{slot}/Q_{cavity} = 0/59$ slpm, 0/136 slpm, and 126/38 slpm. With $Q_{slot}/Q_{cavity} = 0/59$ slpm, regime I and II were present, but regime III was not, and the cavity extinguished. When Q_{cavity} was increased to 136 slpm or when Q_{cavity} decreased to 38 slpm and Q_{slot} was 126 slpm, there was not as much decay in regime II, regime III was much longer in time, and regime IV was suppressed. The results indicated that sufficiently high cavity fueling (either directly into the cavity or through entrainment via the shear layer) could mitigate the decrease in heat release caused by the disruption from the detonation. Furthermore, it was also found that while the *PD* was disruptive to the cavity flow, the high level of energy deposition allowed for ignition across a wider range of T_0 and P_0 in the flowpath when compared to the spark discharge. To wit: the *PD* was capable of igniting the cavity at a T_0 of 500 K, while the spark discharge could not achieve ignition until 570 K for the same pressure and fueling conditions.

The spark discharge also demonstrated similar decreased heat release behavior when using both lower and higher fueling rates. In Fig. 7 with $Q_{slot}/Q_{cavity} = 0/52$ slpm, the heat release process was more gradual, and there were two peaks before the cavity achieved steady burning. The first local peak in heat release came from the first cycling of the cavity after ignition. This preconditioned the cavity for the second heat release peak which was significantly larger. The time between these peaks aligned with the 1–1.5 ms cavity cycling time. Interestingly, when the Q_{cavity} was decreased to 45 slpm and upstream fuel injection ($Q_{slot} = 115$ - slpm) was used, the same multi-peak behavior was present, but there was a lull in emission after the second larger heat release peak. There was then a gradual rise in heat release until steady cavity burning was achieved. This cavity ignition behavior was similar to that with the *PD* where there was a peak in heat release from burning a significant amount of fuel in the cavity followed by a lull

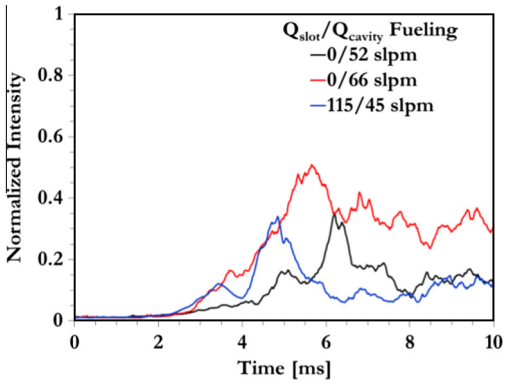

Fig. 7. Average integrated chemiluminescence in cavity during ignition versus time for spark discharge at different Q_{slot} and Q_{cavity}.

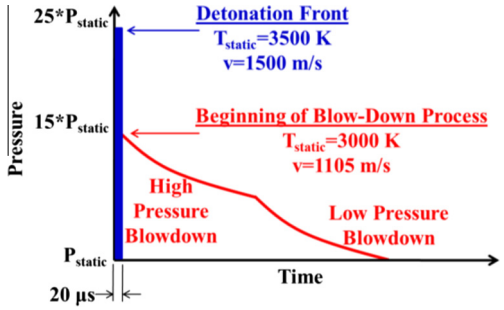

Fig. 8. Initial conditions for *PD* exhaust model.

in heat release. While the exact nature of the spark discharge ignition process was dependent on Q_{cavity}, cavity flame extinction was not observed for the entire range of Q_{cavity} (42–110 slpm) and Q_{slot} (0–126 slpm) employed here.

3.2. Numerical simulations

With the limited set of measurements that were possible to examine the cavity ignition process, numerical simulations were utilized. Here, the focus was on the *PD*. Specifically, an explanation of the decay in heat release after the initial cavity ignition process was sought. Fortunately, a previous investigation of the *PD* exhausting into a M-2 cross-flow provided validation through high-frame-rate shadowgraph and planar laser-induced fluorescence (of NO) [10]. For the simulations, 3-D unsteady calculations using the CFD^{++} code were used [11]. The turbulence was modeled using the two-equation cubic κ-ε model, which has non-linear terms that account for normal-stress anisotropy, swirl, and streamline-curvature effects. Three turbulent Schmidt numbers were employed, $Sc_t = 0.5$, 0.7, and 1.0, to bound the problem and observe any ignition/mixing differences. The detonation and reaction inside the *PD* were not computed [10], but rather the exhaust process was simulated with the boundary conditions shown in Fig. 8. This was reasonable since the majority of the chemical reactions from the *PD* were occurring inside the tube. In order to replicate the products of the detonation from the experiments, the gas composition was derived from the Chapman–Jouguet calculations with the species N_2, H_2O, CO, CO_2, O_2, H_2, O, H, and OH. For the chemical reactions inside the cavity with C_2H_4, the TP2 reduced kinetic model was used and no turbulence-chemistry interaction was taken into account [12]. The computational domain consisted of the full width and height of the test section with a total of 12.4 million cells. The numerical approach was divided into two steps. First a steady-state solution was performed for the supersonic flow path without the interaction of the *PD* tube. Second, the *PD* flow field was initiated at the cavity floor, similar to a shock tube problem. At this time, the simulation was performed in a time-accurate manner.

Initially the simulations were validated in the cavity geometry in terms of capturing the time scales and mixing processes. A comparison of shadowgraph images (integrated) and density gradients (synthetic shadowgraph in the plane of the *PD*) showed some variation across the range of Sc_t (0.5–1.0). Specifically, the computation with $Sc_t = 0.5$ showed too much mixing, while that at $Sc_t = 1.0$ showed too little mixing (relative to experimental observation), therefore bounding the problem. Nevertheless, all three Sc_t were still used for the ignition simulations to see the effect on reactivity. A Sc_t of 0.7 appeared to produce the best agreement with experiments (and also matched the previous validation studies [10]). Figure 9 shows the comparison between the experiments and numerical simulations with no fuel injection. While the early time scales (first 0.12 ms) agreed well, there appeared to be disagreement at later times. Specifically, by 2.8 ms the simulations had relaxed to steady state while the experiments showed the *PD* still exhausting. In fact, the simulations at 1.4 ms agreed with the experiments at 2.8 ms. This result emphasized a deficiency in the *PD* model developed in the previous study [10]: agreement between the simulations and experiment were sought only for the first 0.4 ms where it was most difficult to match the density gradients and plume structure. Consequently, the simulations predicted *PD* blow-down times approximately half that of the experiments. While the initial conditions of pressure, temperature, and velocity of the *PD* model could be adjusted to capture the overall timescale of the exhaust process more accurately, the initial exhaust time scales and structure were in good agreement, and therefore the PD evolution was deemed reasonable for the current ignition simulations.

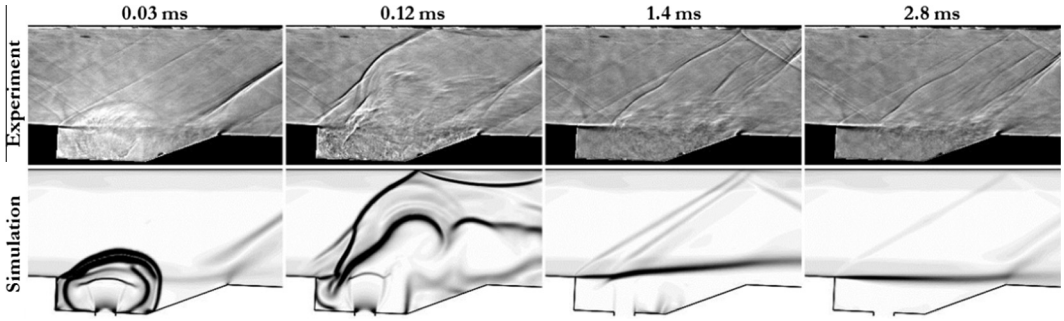

Fig. 9. Comparison of shadowgraph and density gradients from simulations of cavity flow without fueling.

Since there was no direct methodology to compare the chemiluminescence images to the simulations, the time dependence of the T, P (static values) and C_2H_4 mass fraction (Y_{C2H4}) were used to monitor the ignition process. These values were extracted from the numerical simulations in planes at every 6.4 mm spanning the cavity, producing 23 planes. At each time step, the T, P, and Y_{C2H4} were averaged to produce a pseudo-integrated view of the cavity, to compare to the chemiluminescence images of PD ignition in Figs. 5 and 6. For the case with $Q_{slot}/Q_{cavity} = 0/66$ slpm, there was an initial rapid decay of Y_{C2H4} in the cavity. This aligned with regime I in Figs. 5 and 6. Here, the detonation forced a significant amount of C_2H_4 out of the cavity (as shown by inset image (b) above the plot in Fig. 10), and T and P increased because of the elevated values within the detonation plume. In regime II, there were relatively constant values of T, P, and Y_{C2H4} in the cavity. This could be associated with a "cavity ignition delay time" to cycle hot detonation products and ignite the fuel that remained in the cavity. The fuel then started to burn rapidly in regime III with a decrease in Y_{C2H4} and increase in T while maintaining a constant P. The rapid burning in regime III is shown by the deficiency of C_2H_4 in image (c) in Fig. 10 and also by the spike in heat release shown by the increased chemiluminescence in Fig. 5. It is important to note that up to this point the cavity flow had been significantly disrupted by the detonation, specifically by elevated P from the detonation. While this was beneficial to reaction rates to enhance ignition, it was also detrimental because it decreased and, at times, stopped the ramp fueling, since the fuel injection from the closeout ramp was not choked. The simulations were, of course, designed to replicate the experimental fuel injection set-up by defining the fuel mass flow rate and temperature approximately 5 cm upstream of the exit of the fuel injection into the cavity. This location was approximately where the fuel plenum was located, and therefore allowed for pressure variations in the cavity to change Q_{cavity} at the

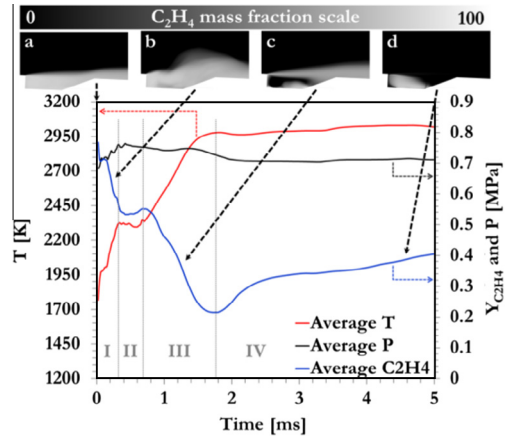

Fig. 10. Psuedo-integrated T, P, and Y_{C2H4} in cavity versus time from simulations with inset simulated images of Y_{C2H4}.

ramp face. Indeed, the approximate 15% increase in the *average* cavity P from the detonation significantly decreased Q_{cavity}. In regimes I, II, and III, Q_{cavity} was reduced, the cavity cycling and flow was significantly disrupted, and the detonation was able to ignite and burn most of the fuel within the cavity. This led to decreased heat release in regime IV because most of the fuel and air were consumed and there was not sufficient time to replenish a reactive mixture. Simultaneously, the PD was at the end of its exhaust cycle, and thus P began to decrease in the cavity. This in turn (i) allowed for more fuel to flow into the cavity as shown in regime IV of Fig. 10 and after a period of time (ii) increased heat release and chemiluminescence as shown in Fig. 5. After a few milliseconds, the cavity flow was able to cycle a few times and regain its normal steady state burning. Image (d) in Fig. 10 shows this behavior with a distribution of fuel throughout the cavity front, along the floor, and near the leading edge of the shear layer. As noted above, the time scales differed by a factor of ~2, due to the PD behaviors (simulated vs. observed). Nevertheless, the overall

trends were correctly captured and gave insight into mechanisms for the observed ignition regimes. The high-pressure of the detonation with several milliseconds of duration disrupted the cavity flow and the non-choked fuel injection led to less fuel.

4. Summary and conclusions

Cavity ignition in a supersonic flow was achieved using two vastly different forms of energy deposition devices that caused different levels of flow disruption. Spark discharge ignition was a more passive process, following the flow to achieve steady cavity burning. Conversely, *PD* ignition was extremely disruptive to the cavity flow dynamics with its high-pressure and -temperature plume. The disruption was found to be advantageous under certain conditions (such as at lower T_0 and P_0), but was also seen to be somewhat detrimental because of decreased cavity burning and near extinction from the flow field interaction. High-frame-rate shadowgraph and chemiluminescence imaging allowed for an unprecedented look at the transient ignition process and provided a means for comparison to simulations. While the simple model developed of the *PD* exhaust process predicted shorter time scales, it correctly captured all burning regimes of the ignition process observed in the experiments. Most importantly, it provided insight to the mechanism of decreased heat release because of the high-pressure *PD* exhaust momentarily diminishing fuel flow to the cavity. Therefore, a smaller *PD* with shorter blow-down time that produces less pressure rise in the cavity, as well choked fuel injection to the cavity has the potential to mitigate any decrease in burning and therefore a greater chance for successful ignition over a wide range of conditions.

Acknowledgements

This work was partially supported by the Air Force Office of Scientific Research under Dr. Chiping Li.

References

[1] M.R. Gruber, R.A. Baurle, T. Mathur, K.-Y. Hsu, *J. Propul. Power* 17 (1) (2001) 146–153.
[2] M.R. Gruber, J.M. Donbar, C.D. Carter, K.-Y. Hsu, *J. Propul. Power* 20 (5) (2004) 769–778.
[3] S.B. Leonov, D.A. Yarantsev, A.P. Napartovich, I.V. Kochetov, 44th AIAA Aerospace Sciences Meeting, Reno, Nevada, AIAA-2006-563, 2006.
[4] H. Do, M.A. Cappelli, M.G. Mungal, *Combust. Flame* 157 (9) (2010) 1783–1794.
[5] T.C. Wagner, W.F. O'Brien, G.B. Northam, J.M. Eggers, *J. Propul. Power* 5 (5) (1989) 548–554.
[6] Y. Sato, M. Sayama, K. Ohwaki, et al., *J. Propul. Power* 8 (4) (1992) 883–889.
[7] L.S. Jacobsen, C.D. Carter, R.A. Baurle, et al., *J. Propul. Power* 24 (4) (2008) 641–654.
[8] S. Tabejamaat, Y. Ju, T. Niioka, *AIAA J.* 35 (9) (1997) 1441–1447.
[9] M.R. Gruber, A.S. Nejad, 32nd AIAA Aerospace Sciences Meeting, AIAA-94-0544.
[10] T. Ombrello, C.D. Carter, J. McCall, F. Schauer, C.-J. Tam, A. Naples, J. Hoke, K.-Y. Hsu, 50th AIAA Aerospace Sciences Meeting, AIAA-2012-123.
[11] Metacomp Technologies, http://www.metacomptech.com/index.html, 2009.
[12] J. Liu, C.-J. Tam, T. Lu, C.K. Law, 42nd Joint Propulsion Conference, AIAA 2006-4862.